CHINESE OPTICS LETTERS

Vol. 19, No. 5 | May 2021

Multi-focus optical fiber lens based on all-dielectric metasurface

Xingyu Zhang (张星宇)[1], Chunying Guan (关春颖)[1*], Keda Wang (王可达)[1], Lin Cheng (程 琳)[1], Jing Yang (杨 菁)[1**], Jinhui Shi (史金辉)[1], Hongchao Liu (刘宏超)[2], Zhihai Liu (刘志海)[1], and Libo Yuan (苑立波)[3]

[1] Key Laboratory of In-Fiber Integrated Optics of Ministry of Education, College of Physics and Optoelectronic Engineering, Harbin Engineering University, Harbin 150001, China

[2] Institute of Applied Physics and Materials Engineering, University of Macau, Avenida da Universidade, Taipa, Macao SAR, China

[3] Photonics Research Center, Guilin University of Electronics Technology, Guilin 541004, China

*Corresponding author: cyguan@163.com

**Corresponding author: yangjing13@hrbeu.edu.cn

Received October 1, 2020 | Accepted November 8, 2020 | Posted Online February 20, 2021

A multi-focus optical fiber lens is numerically demonstrated based on an all-dielectric metasurface structure. The metasurface consists of an array of rectangular silicon resonators with varying widths in order to obtain the required phase distribution. The core diameter of the multimode fiber is large enough to contain sufficient resonance units. The spatial distribution of the dielectric resonators is dictated by spatial multiplexing, including interleaving meta-atoms and lens aperture division, to achieve multi-focus properties. The proposed optical fiber metalens can produce two or three focal points along the longitudinal direction with high focusing efficiency. The size of every focal point is close to the diffraction limit, and the relative intensity on each focus can be controlled by adjusting the number of the respective resonators. The proposed optical fiber lens will have a great potential in the fields of integrated optics and multifunctional micro/nano devices.

Keywords: multi-focus lens; optical fiber; metasurface.
DOI: 10.3788/COL202119.050601

1. Introduction

A refractive optical device is one of the most important optical elements in optical systems that can manipulate light beams such as focusing, deflecting, and reflecting. The change of the wavefront of a beam is mainly caused by the cumulative phase of light passing through a medium over a distance. Consequently, the sizes of the refractive optical elements are usually much larger than the light wavelength, which limits the optical device miniaturization. Metamaterials, as a new kind of three-dimensional (3D) material that can be artificially designed and manufactured, exhibit exotic properties beyond natural materials and offer an opportunity to reduce greatly the sizes of beam shaping elements[1]. However, the structures of 3D metamaterials are complex, and their manufacturing processes are relatively difficult. Metasurfaces, as the two-dimensional (2D) counterpart of metamaterials, not only have excellent optical properties, but also have consistent fabrication techniques with current micromachining technologies. Metasurfaces have ultrathin optical structures composed of subwavelength resonant elements on the 2D planes. By changing the shape, size, material, and spatial arrangement of the resonant elements, the amplitude, phase, and polarization of the beam can be fully controlled by the metasurfaces[2–5]. Plasmonic metasurfaces demonstrated important applications in the perfect absorber, beam focusing, anomalous refraction, and reflection[6–9]. A metal–graphene hybrid metasurface is designed to realize the tunable polarization conversion[10]. However, due to inherent losses of metal, the optical efficiency of plasmonic metasurfaces is low. In contrast, all-dielectric metasurfaces have low losses and high transmission efficiency, which thereby have attracted much more attention. Among them, the metasurface based on the Pancharatnam–Berry (P-B) phase would realize 2π phase modulation and generate an arbitrary wavefront[11–13]. Such phase modulation depends on the orientations of the resonators rather than the size and shape. However, P-B phase-based metasurfaces are only sensitive to circularly polarized light; therefore, they are limited in some optical applications. Dielectric metasurfaces based on Mie resonance not only have high transmission efficiency but also are sensitive to light with an arbitrary polarization direction. When a beam propagates through the dielectric elements with high

refractive index, the electric and magnetic dipole resonances will occur and affect the scattering of the beam. They have been demonstrated to manipulate the phase[14–18], polarization[19,20], and amplitude of the scattered light via spatially and geometrically engineered resonators. In the past few years, all-dielectric metasurfaces have been used to design a variety of optical devices, including absorbers[21,22], and optical controls for nanostructured macroscopic objects[23] and computer generated holograms[24,25]. At the same time, many dielectric metasurfaces have been used for focusing close to the diffraction limit[26,27]. Multi-focus lenses have potential applications in optical communication, optical imaging, optical data storage, and optical manipulation. However, the multi-focal metasurface only attracts little attention. According to the focus direction, the multi-focus lenses were divided into transverse focus lenses[28–31] and longitudinal focus lenses[12,32–35]. Most of these multi-focus lenses have been designed in terms of the P-B phase. Recently, a multi-foci metalens with polarization-rotated focal points has been proposed[36], but it only works for circularly polarized light. Therefore, when incident light is linearly polarized, its focusing efficiency will not exceed 50%. In addition, a tunable metasurface proposed by Yilmaz *et al.* achieves multi-focus beams through a complex two-layer structure[35]. As a general optical waveguide, optical fibers have some advantages, such as immunity to electromagnetic interference, lightweight, flexibility, and long transmission distance. Therefore, optical fiber-based microstructures have displayed a variety of interesting functions, such as optical fiber microphones[37], delivery of orbital angular momentum light[38], shaping of spatial beams[39–42], and polarization conversion[43]. The metasurface on the end face of the optical fiber can avoid the use of alignment devices, which is convenient to the integration of the optical system and greatly reduces the volume of the optical system.

In this work, we propose a multi-focus and multimode fiber lens with a dielectric metasurface. The full 2π phase modulation is realized by using a single rectangular dielectric resonator (RDR). The distribution of resonant elements is designed by spatial multiplexing, including interleaving meta-atoms and lens aperture division, to achieve the focal points with different focal lengths. When the beam is incident from the optical fiber to the metasurface, it produces different additional phase distributions and achieves multi-focal points along the longitudinal direction. The relative intensity of each focal point is controllable by adjusting the numbers of RDRs that contribute to this focus. The multi-focus lens can achieve clear images at multiple focal planes. In addition, our multi-focus metalens will have advantages in nanoparticle manipulation, optical data storage, and optical information processing.

2. Design Principles of the Optical Fiber Lens

The core size of the single mode fiber is too small to maintain enough numbers of resonance units, so spatial multiplexing is difficult to achieve. By contrast, the core diameter of the multimode fiber is large enough to contain sufficient resonance units. Therefore, the multimode fiber is employed here. The proposed optical fiber lens has a metasurface structure. The rectangular amorphous silicon (α-Si) resonators are patterned as meta-atoms on the end face of the multimode optical fiber. As shown in Fig. 1(a), the multimode fiber lens can converge an incident beam into multiple focal points, where the diameter D of the fiber core is 62.5 μm. In order to obtain a focused beam, the spatial phase distribution in the end face of the optical fiber must satisfy the following equation:

$$\varphi(x) = 2m\pi - \frac{2\pi}{\lambda}\left(\sqrt{x^2+f^2} - f\right), \tag{1}$$

where m is a positive integer, x is the distance between the resonant element and the core center, f is the focal length, and λ is the wavelength of the incident beam. As long as the wavelength λ and the focal length f are determined, the phase distribution curve of the optical fiber lens can be obtained. In order to realize a full 2π phase modulation, an RDR is chosen. As shown in Fig. 1(b), the RDR locates at the center of the unit cell, where the period of the unit cell is $S = 500$ nm, the height H of the RDR is 600 nm, and the working wavelength of the fiber lens is 1300 nm. The refractive indexes of α-Si and the fiber core are 3.522 and 1.46, respectively. Figure 1(c) shows the relationship between the additional phase and transmittance of the transmitted light and the width W of an RDR. The simulation is calculated by the 2D finite difference time domain (FDTD)

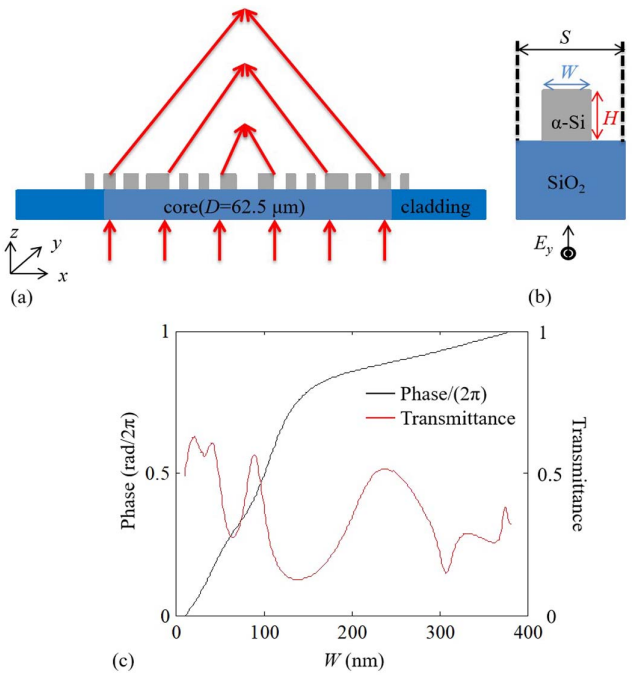

Fig. 1. (a) Schematic of multi-focus optical fiber metalens. (b) Schematic of a unit cell composed of a single RDR. The light is incident from the fiber, and the polarization is along the y direction. (c) The phase (black line) and transmittance (red line) variations of the transmitted light with the width W of single RDR.

method, where the polarization of the incident beam is along the long side of the RDR (y direction). When the width W of the RDR varies from 50 to 400 nm, the full 2π phase modulation can be achieved.

Firstly, the single focus fiber lens with the focal length of 100 μm is numerically demonstrated. The additional phase distribution of RDRs along the x direction should satisfy the phase function in Eq. (1). Thus, as long as the focal length of the fiber lens is determined, the width of each RDR can be calculated according to Fig. 1(c). As shown in Fig. 2(a), the solid line denotes the phase distribution curve calculated by Eq. (1) when the focal length is 100 μm, and the blue points are the designed phases of each RDR simulated by FDTD. The field monitor was placed 200 nm away from the surface of the RDR, and the phases were calculated at the middle position of each RDR. The intensity distribution of the fiber lens in the x–z plane is shown in Fig. 2(b). An obvious focus is obtained at the distance of 100 μm away from the fiber end. It can be seen that the calculated result is in a good agreement with the expected result, which verifies the correctness of the single RDR simulation result. Figure 2(c) shows the light intensity distribution on the focal plane. The full-width-at-half-maximum (FWHM) of the light intensity at the focal point is about 2.61 μm, which is close to the diffraction limit calculated by the diffraction formula,

$$d = 1.22\lambda f / D, \tag{2}$$

where D is the aperture of the optical fiber lens. According to Eq. (2), the diffraction limit is 2.54 μm. In addition, the focusing efficiency is as high as 65.9%, indicating that the optical fiber lens has high transmission efficiency. The focusing efficiency is defined as the measured power in the focus plane with a radius equal to three times the FWHM spot size divided by the total incident power[44]. The polarization of the transmitted light is consistent with that of the incident light.

In order to achieve multi-focal functionality, the phase distribution functions corresponding to different focal points need to be satisfied simultaneously. Spatial division multiplexing, including the interleaving meta-atoms and the lens aperture division, is applied to obtain different phase distribution functions. The interleaving meta-atoms method refers to the alternate arrangement of the RDR contributing to different focal lengths, while the lens aperture division method refers to dividing optical fiber lens into several regions, and then placing multiple RDRs with the same focal length into each region. Here, the dual-focus fiber lenses with focal lengths of 50 and 100 μm are demonstrated below. The discretized phase distributions from the interleaving meta-atoms method and lens aperture division method are presented in Figs. 3(a) and 3(b), respectively. The solid lines are the phase curves calculated for the focal lengths of 50 and 100 μm according to Eq. (1), and the blue solid points are the positions of the RDRs and the discretized phases of the two methods. The positions of the RDRs are determined by the period. As shown in Fig. 3(a), the positions of the RDRs are chosen alternately on the phase curves of 50 and 100 μm. The fundamental mode of the fiber has a Gaussian profile; therefore, the number of the RDRs contributing to the two focal points is not divided equally. In order to obtain the same intensity at two focal points, the RDRs near the core edge of the fiber are only selected on the phase curve of 100 μm to compensate for the light intensity at the focal point of 100 μm. The intensity ratio between two focal points can be adjusted by using the number of the respective RDRs. Similarly, for the lens aperture division method, as shown in Fig. 3(b), the phase distribution at the focal point of 50 μm can be realized based on the RDRs at the middle core region, and the rest of the RDRs in the outer core region contribute to the focal point at 100 μm. By adjusting the size of the two regions, i.e., the amount of RDRs acting on different focal points, the intensity ratio between the two focal points can also be engineered.

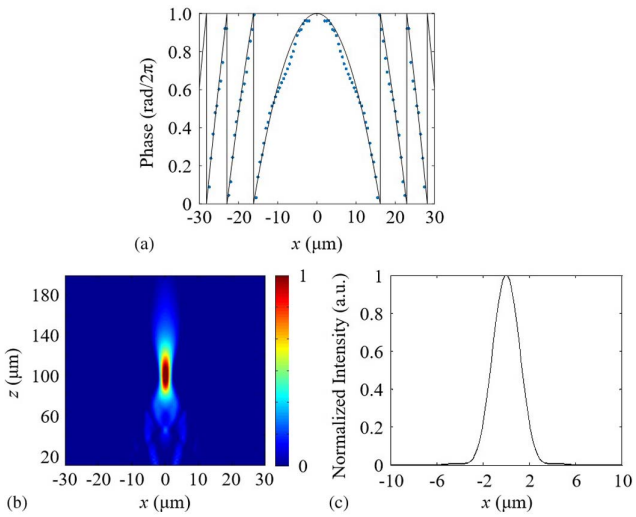

Fig. 2. (a) Phase distributions of the fiber lens. Solid line: analytical phase of the lens with its focal length of 100 μm. Blue points: digitized phase profile based on FDTD simulation. (b) Calculated intensity distribution of the fiber lens with the focal length of 100 μm in the x–z plane. (c) The intensity profile across the focal plane ($z = 100$ μm) of the fiber lens.

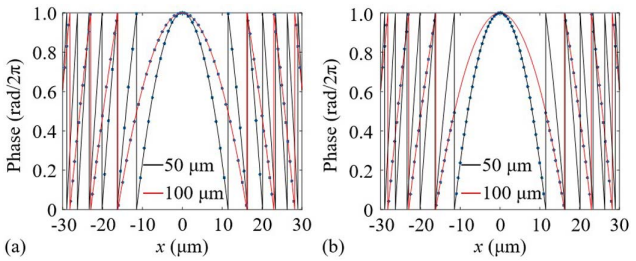

Fig. 3. Discretized phase distributions based on (a) interleaving meta-atoms and (b) lens aperture division methods for the focal lengths of 50 and 100 μm. Solid lines: analytical phases. Blue points: the positions and discretized phases of RDRs used in the calculation.

3. Simulation Results of the Optical Fiber Lens

Suppose linearly polarized Gaussian light is incident from the core of the multimode fiber upon the all-dielectric metasurface lens. The light intensity distributions on the x–z plane of the bifocal fiber lenses designed by interleaving meta-atoms and lens aperture division are shown in Figs. 4(a) and 4(d), respectively. Two obvious focal points are observed at the distances of 50 and 100 μm away from the fiber lens. The simulation results are consistent with the designed lens. The field profiles along the z-axis direction are shown in Figs. 4(b) and 4(e). The maximum light intensities at the two focal points are approximately equal. The depth of the focus at far focal point is longer than that at the near focal point. The light intensity profiles on the focal planes along the x axis are shown in Figs. 4(c) and 4(f). The FWHMs of the 50 and 100 μm lenses are 1.81 and 2.61 μm based on the interleaving meta-atoms, while those of the lenses are 2.21 and 2.61 μm based on the lens aperture division. Both of them are close to their respective diffraction limits of 1.269 and 2.538 μm calculated by Eq. (2). The focusing efficiencies of the optical fiber lens designed by interleaving meta-atoms are 46.7% and 54.3% at two focal points, respectively, while those of the metasurface lens designed by aperture division are 52.0% and 57.6%, respectively. Although the maximum light intensities of the two focal points on the focal plane are almost equal, the far focal point has a larger FWHM, and its focusing efficiency is relatively high. Compared with the interleaving meta-atoms method, the background scattering light for the lens aperture division method is more obvious; therefore, the FWHM is relatively wide.

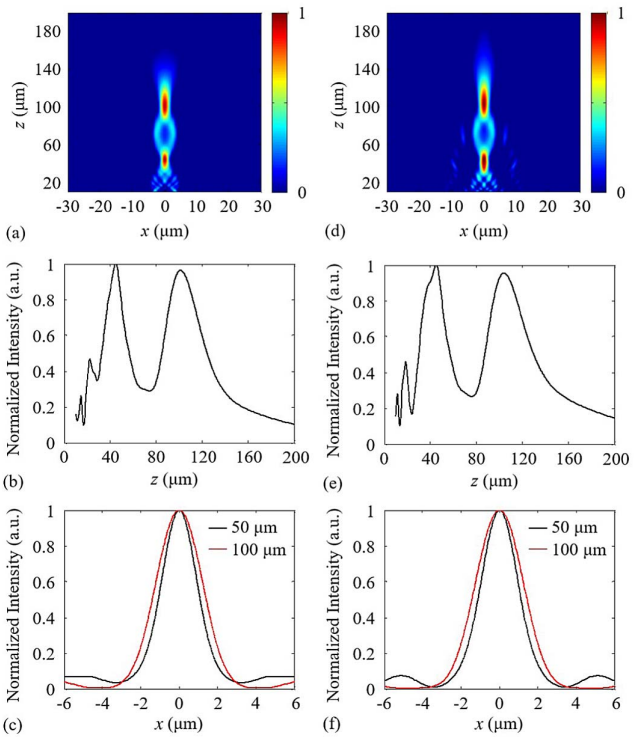

Fig. 4. Intensity distributions of bifocal fiber lenses designed by (a)–(c) interleaving meta-atoms and (d)–(f) lens aperture division. The intensity distributions (a), (d) in the x–z plane, (b), (e) along the z axis, and (c), (f) at the focal plane ($z = 50$ and 100 μm).

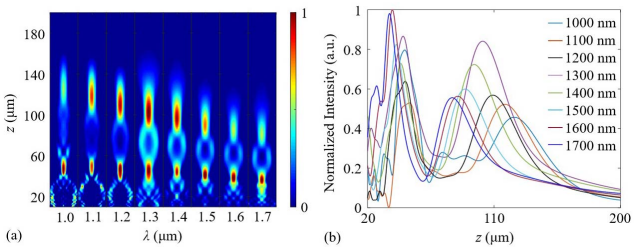

Fig. 5. Intensity distributions of bifocal fiber lens based on interleaving meta-atoms for different incident wavelengths. The intensity distributions (a) in the x–z plane and (b) along the z axis.

For the different incident wavelengths, the field intensity distributions of the bifocal fiber lens based on the interleaving meta-atoms are shown in Fig. 5. The wavelength of incident light ranges from 1000 to 1700 nm. When the fiber lens is incident with broadband light, there are still two clear focal points in the far field. As shown in Fig. 5(a), the focal length for the distant focus decreases obviously as the wavelength increases, while that for the near focus changes slightly. The energy ratio between the two focal points changes, and more energy is focused at the near focal point as the wavelength deviates from the optimized wavelength of 1300 nm. The calculated results indicate that the proposed optical fiber lens can realize broadband multi-focal focusing.

A three-focus optical fiber lens with the focal lengths of 53, 83, and 138 μm is also demonstrated, and the calculated result is shown in Fig. 6. The focusing efficiencies of the three foci are 45.8%, 52.5%, and 55.1%, respectively. As the number of the focal points increases, the focusing efficiency of each focal point decreases. In addition, the background scattered light becomes relatively strong. The RDRs not only contribute to one specific focal point but also cause background noises at other focal points. The FWHMs of the three focal points are 2.207, 3.411, and 5.819 μm, respectively, which are larger than those of single and double-focus lenses. Meanwhile, the calculated focal lengths

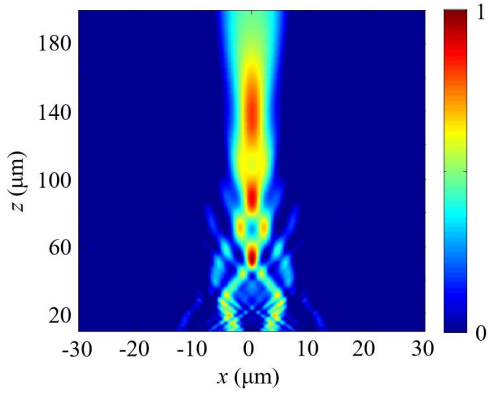

Fig. 6. Intensity distribution of three-focus fiber lens.

of the three focal points are also shorter than the design values. Since the size of the end face of the optical fiber lens remains unchanged, with the increase of the focal points, the number of the RDRs for each focal point will become smaller, thus affecting the focusing performance.

4. Conclusion

In summary, we numerically demonstrate a multi-focal optical fiber metasurface lens designed by interleaving meta-atoms and lens aperture division. A metasurface with RDRs is designed on the end surface of the multimode fiber. Multiple focal points can be generated in the axial direction. The focal lengths are close to the predicted values. The focusing efficiencies of the optical fiber lens are relatively high, and the FWHMs of the foci are close to the diffraction limit. The optical fiber lens can not only achieve multi-focus functionality at a single wavelength, but also maintain multiple foci across the broad wavelength range. The multi-focus optical lens can achieve a tunable response if the RDRs are composed of thermo-optical or electro-optical materials. The combination of the optical fiber and metasurface can avoid the use of alignment devices in optical systems and is more convenient to optical integration. The multi-focus provides a new way for optical capturing and holographic imaging.

Acknowledgement

This work was supported by the National Natural Science Foundation of China (NSFC) (Nos. 91750107, 61675054, and U1931121), Natural Science Foundation of Heilongjiang Province, China (Nos. ZD2018015 and ZD2020F002), 111 Project of the Harbin Engineering University (No. B13015), and Fundamental Research Funds for Harbin Engineering University of China (Nos. 3072020CFT2504 and 3072020CFT2501).

References

1. S. Jahani and Z. Jacob, "All-dielectric metamaterials," Nat. Nanotechnol. **11**, 23 (2016).
2. H. H. Hsiao, C. H. Chu, and D. P. Tsai, "Fundamentals and applications of metasurfaces," Small Methods **1**, 1600064 (2017).
3. P. Genevet, F. Capasso, F. Aieta, M. Khorasaninejad, and R. Devlin, "Recent advances in planar optics: from plasmonic to dielectric metasurfaces," Optica **4**, 139 (2017).
4. A. V. Kildishev, A. Boltasseva, and V. M. Shalaev, "Planar photonics with metasurfaces," Science **339**, 1232009 (2013).
5. C. Choi, S. Kim, J. Yun, J. Sung, S. Lee, and B. Lee, "Deflection angle switching with a metasurface based on phase-change nanorods," Chin. Opt. Lett. **16**, 050009 (2018).
6. P. Qiu, D. Zhang, M. Jing, T. Lu, B. Yu, Q. Zhan, and S. Zhuang, "Dynamic tailoring of surface plasmon polaritons through incident angle modulation," Opt. Express **26**, 9772 (2018).
7. L. Yin, T. Huang, F. Han, J. Liu, and P. Liu, "Terahertz multichannel metasurfaces with sparse unit cells," Opt. Lett. **44**, 1556 (2019).
8. N. Muhammad, T. Fu, Q. Liu, X. Tang, Z. Deng, and Z. Ouyang, "Plasmonic metasurface absorber based on electro-optic substrate for energy harvesting," Materials **11**, 2315 (2018).
9. C. Saeidi and D. Weide, "Wideband plasmonic focusing metasurfaces," Appl. Phys. Lett. **105**, 053107 (2014).
10. J. Huang, T. Fu, H. Li, Z. Shou, and X. Gao, "A reconfigurable terahertz polarization converter based on metal–graphene hybrid metasurface," Chin. Opt. Lett. **18**, 013102 (2020).
11. M. Khorasaninejad, W. T. Chen, R. C. Devlin, J. Oh, A. Y. Zhu, and F. Capasso, "Metalenses at visible wavelengths: diffraction-limited focusing and subwavelength resolution imaging," Science **352**, 1190 (2016).
12. Q. Chen, Y. Li, Y. Han, D. Deng, D. Yang, Y. Zhang, Y. Liu, and J. Gao, "High numerical aperture multifocal metalens based on Pancharatnam–Berry phase optical elements," Appl. Opt. **57**, 7891 (2018).
13. R. Lin and X. Li, "Multifocal metalens based on multilayer Pancharatnam–Berry phase elements architecture," Opt. Lett. **44**, 2819 (2019).
14. M. I. Shalaev, J. Sun, A. Tsukernik, A. Pandey, K. Nikolskiy, and N. M. Litchinitser, "High-efficiency all-dielectric metasurface for ultracompact beam manipulation in transmisson mode," Nano Lett. **15**, 6261 (2015).
15. Y. F. Yu, A. Y. Zhu, R. Paniagua-Domínguez, Y. H. Fu, B. Luk'yanchuk, and A. I. Kuznetsov, "High-transmission dielectric metasurface with 2π phase control at visible wavelengths," Laser Photon. Rev. **9**, 412 (2015).
16. J. Xu, M. Cua, H. Zhou, Y. Horie, A. Faraon, and C. Yang, "Wide-angular-range and high-resolution beam steering by a metasurface-coupled phased array," Opt. Lett. **43**, 5255 (2018).
17. S. Kruk, F. Ferreira, N. M. Suibhne, C. Tsekrekos, I. Kravchenko, A. Ellis, D. Neshev, S. Turitsyn, and Y. Kivshar, "Transparent dielectric metasurfaces for spatial mode multiplexing," Laser Photon. Rev. **12**, 1800031 (2018).
18. A. Özdemir, N. Yilmaz, S. A. Alboon, Y. Takashima, and H. Kurt, "Analysis of the focusing crosstalk effects of broadband all-dielectric planar metasurface microlens arrays for ultra-compact optical device applications," OSA Continuum **1**, 506 (2018).
19. S. Kruk, B. Hopkins, I. I. Kravchenko, A. Miroshnichenko, D. N. Neshev, and Y. S. Kivshar, "Invited article: broadband highly efficient dielectric metadevices for polarization control," APL Photon. **1**, 030801 (2016).
20. J. Hu, X. Zhao, Y. Lin, A. Zhu, X. Zhu, P. Guo, B. Cao, and C. Wang, "All-dielectric metasurface circular dichroism waveplate," Sci. Rep. **7**, 41893 (2017).
21. W. Zhu, F. Xiao, M. Kang, and M. Premaratne, "Coherent perfect absorption in an all-dielectric metasurface," Appl. Phys. Lett. **108**, 121901 (2016).
22. X. Liu, K. Fan, I. V. Shadrivov, and W. J. Padilla, "Experimental realization of a terahertz all-dielectric metasurface absorber," Opt. Express **25**, 191 (2017).
23. O. Ilic and H. A. Atwater, "Self-stabilizing photonic levitation and propulsion of nanostructured macroscopic objects," Nat. Photon. **13**, 289 (2019).
24. W. Freese, T. Kämpfe, W. Rockstroh, E. B. Kley, and A. Tünnermann, "Optimized electron beam writing strategy for fabricating computer-generated holograms based on an effective medium approach," Opt. Express **19**, 8684 (2011).
25. W. Yu, K. Takahara, T. Konishi, T. Yotsuya, and Y. Ichioka, "Fabrication of multilevel phase computer-generated hologram elements based on effective medium theory," Appl. Opt. **39**, 3531 (2000).
26. W. Chen, A. Y. Zhu, V. Sanjeev, M. Khorasaninejad, Z. Shi, E. Lee, and F. Capasso, "A broadband achromatic metalens for focusing and imaging in the visible," Nat. Nanotechnol. **13**, 220 (2018).
27. P. R. West, J. L. Stewart, A. V. Kildishev, V. M. Shalaev, V. V. Shkunov, F. Strohkendl, Y. A. Zakharenkov, R. K. Dodds, and R. Byren, "All-dielectric subwavelength metasurface focusing lens," Opt. Express **22**, 26212 (2014).
28. Y. Wang, C. Guan, X. Ding, K. Zhang, B. Ratni, S. N. Burokur, X. Gu, and Q. Wu, "Multi-focus hologram utilizing Pancharatnam–Berry phase elements based metamirror," Opt. Lett. **44**, 2189 (2019).
29. J. He, J. Ye, X. Wang, Q. Kan, and Y. Zhang, "A broadband terahertz ultrathin multi-focus lens," Sci. Rep. **6**, 28800 (2016).
30. Y. Ma, G. Rui, B. Gu, and Y. Cui, "Trapping and manipulation of nanoparticles using multifocal optical vortex metalens," Sci. Rep. **7**, 14611 (2017).
31. P. Li, X. Guo, S. Qi, L. Han, Y. Zhang, S. Liu, Y. Li, and J. Zhao, "Creation of independently controllable multiple focal spots from segmented Pancharatnam–Berry phases," Sci. Rep. **8**, 9831 (2018).
32. X. Chen, M. Chen, M. Q. Mehmood, D. Wen, F. Yue, C. W. Qiu, and S. Zhang, "Longitudinal multifoci metalens for circularly polarized light," Adv. Opt. Mater. **3**, 1201 (2015).

33. W. Wang, Z. Guo, K. Zhou, Y. Sun, F. Shen, Y. Li, S. Qu, and S. Liu, "Polarization-independent longitudinal multi-focusing metalens," Opt. Express **23**, 29855 (2015).
34. S. Tian, H. Guo, J. Hu, and S. Zhuang, "Dielectric longitudinal bifocal metalens with adjustable intensity and high focusing efficiency," Opt. Express **27**, 680 (2019).
35. N. Yilmaz, A. Ozdemir, A. Ozer, and H. Kurt, "Rotationally tunable polarization-insensitive single and multifocal metasurface," J. Opt. **21**, 045105 (2019).
36. X. Zang, H. Ding, Y. Intaravanne, L. Chen, Y. Peng, J. Xie, Q. Ke, A. V. Balakin, A. P. Shkurinov, X. Chen, Y. Zhu, and S. Zhuang, "A multi-foci metalens with polarization-rotated focal points," Laser Photon. Rev. **13**, 1900182 (2019).
37. H. Wang, Z. Xie, M. Zhang, H. Cui, J. He, S. Feng, X. Wang, W. Sun, J. Ye, P. Han, and Y. Zhang, "A miniaturized optical fiber microphone with concentric nanorings grating and microsprings structured diaphragm," Opt. Laser Technol. **78**, 110 (2016).
38. K. Weber, F. Hütt, S. Thiele, T. Gissibl, A. Herkommer, and H. Giessen, "Single mode fiber based delivery of OAM light by 3D direct laser writing," Opt. Express **25**, 19672 (2017).
39. T. Gissibl, M. Schmid, and H. Giessen, "Spatial beam intensity shaping using phase masks on single-mode optical fibers fabricated by femtosecond direct laser writing," Optica **3**, 448 (2016).
40. A. Koshelev, G. Calafiore, C. Piña-Hernandez, F. I. Allen, S. Dhuey, S. Sassolini, E. Wong, P. Lum, K. Munechika, and S. Cabrini, "High refractive index Fresnel lens on a fiber fabricated by nanoimprint lithography for immersion applications," Opt. Lett. **41**, 3423 (2016).
41. J. Yang, I. Ghimire, P. C. Wu, S. Gurung, C. Arndt, D. P. Tsai, and H. W. H. Lee, "Photonic crystal fiber metalens," Nanophotonics **8**, 443 (2019).
42. M. Principe, M. Consales, A. Micco, A. Crescitelli, G. Castaldi, E. Esposito, V. L. Ferrara, A. Cutolo, V. Galdi, and A. Cusano, "Optical fiber meta-tips," Light: Sci. Appl. **6**, e16226 (2017).
43. T. Liu, S. Yang, D. Tang, H. Da, R. Feng, T. Zhu, F. Sun, and W. Ding, "Polarization conversion based on an all-dielectric metasurface for optical fiber applications," J. Phys. D **50**, 334001 (2017).
44. A. Arbabi, Y. Horie, A. J. Ball, M. Bagheri, and A. Faraon, "Subwavelength-thick lenses with high numerical apertures and large efficiency based on high-contrast transmitarrays," Nat. Commun. **6**, 7069 (2015).